Filling the THz gap—high power sources and applications

2006 Rep. Prog. Phys. 69 301

(http://iopscience.iop.org/0034-4885/69/2/R01)

INSTITUTE OF PHYSICS PUBLISHING REPORTS ON PROGRESS IN PHYSICS

Rep. Prog. Phys. **69** (2006) 301–326 doi:10.1088/0034-4885/69/2/R01

Filling the THz gap—high power sources and applications

Gwyn P Williams

Jefferson Lab, 12000 Jefferson Avenue, Newport News VA 23606, USA

Received 8 August 2005, in final form 1 November 2005
Published 5 December 2005
Online at stacks.iop.org/RoPP/69/301

Abstract

Electromagnetic waves centred at a frequency of 1 THz lie between photonics on the one hand and electronics on the other, and are very hard to generate and detect. However, since the THz part of the spectrum is energetically equivalent to many important physical, chemical and biological processes including superconducting gaps and protein dynamical processes, it is of great interest to facilitate experimental research in this region. This has stimulated major steps in the past decade for filling this gap in the usable spectrum. In this review paper we describe the evolution of a new generation of sources that boost the average power available in the THz region by more than a million-fold, making this region routinely accessible for the first time. This is achieved using two enhancement factors, namely relativistic electrons and super-radiance. We will also point to the scientific potential for discovery that is now enabled in this region.

(Some figures in this article are in colour only in the electronic version)

Contents

1. Introduction to the electromagnetic spectrum and the fundamental physical reasons for the existence of the THz gap

To set this paper in context, this review discusses the development of high power THz sources, where high power is defined as being an average power of 10 W or greater, with peak powers of a Megawatt or more.

THz lies between photonics and electronics as illustrated in the electromagnetic spectrum shown in the bar graph of figure 1. The visible part of the electromagnetic spectrum is familiar to us, and contains the colours of light with which most of us are familiar. Within this visible spectrum, red has a longer wavelength than blue, and red also corresponds to a lower frequency of oscillation. Towards higher frequencies are ultraviolet, x-rays, then gamma rays, while in the other direction, at lower frequencies come infrared, far-infrared, microwaves, radar and radio waves. The study of visible light is sometimes called photonics, the sources being light bulbs and lasers. Electromagnetic waves at much lower frequencies are usually generated in a different way, using electronics and oscillators. In between these two regions lies a part of the spectrum which is more difficult both to make and detect. We are speaking of light in the far-infrared, whose frequencies lie in the region from 0.1–10 THz, and whose wavelengths are from 3 mm to 30 μm.

In the THz range, a normal 1400 K black body source puts merely nanowatts of power over the entire THz range onto a typical sample, due to Planck's radiation law. From the electronics side, the power from oscillators goes down with increasing frequency. These points are shown in figure 2 which clearly shows the drop in power from both the electronic and photonic sides and hence illustrates the difficulties associated with making high power in the THz region.

Even though this paper focuses on high power sources, to establish the context, we note that other sources for this region have been, and are, important for most THz applications. Historically, Hg lamps, in conjunction with Michelson interferometers and liquid helium cooled bolometric detectors, were the mainstay of far-infrared spectroscopy, as THz was called for over a century. Recently, Auston switches [1] and their derivatives have been developed commercially and can produce up to 1 mW of broadband THz light. They are now seeing extensive use. Quantum cascade lasers [2] are being actively developed, and are likely to produce tens of mW into a narrow band in the THz region. An excellent review of laboratory-based sources was prepared recently in an article by Ferguson and Zhang [3].

However, none of the above comes into our earlier definition of high power THz, and for this we turn to a different technology, namely synchrotron radiation from particle accelerators. A pioneering example of this type of source is the free electron laser (FEL) at Santa Barbara, USA [4], which is highly tunable, and has done pioneering work in many areas over an extensive and highly productive period that still continues. This source has peak powers in the tens of kilowatts regime. More recently we are seeing the advent of much higher power at newer, large facilities, some operating in dedicated and some in parasitic mode. In the future it will be possible to scale this technology substantially down in size.

2. General introduction to methods for the production of light from accelerators

Critical to the success of high power THz light generation are two concepts. The first is the use of relativistic electrons to enhance the propagating electromagnetic fields [5–8], and the second is the use of super-radiance [9, 10] in which many electrons radiate in phase with each other. Both of these will be explained in detail in the following section. Converting these concepts into practical high power THz sources has a long history of concomitant development of particle accelerators and their associated technologies, and of calculations and applications

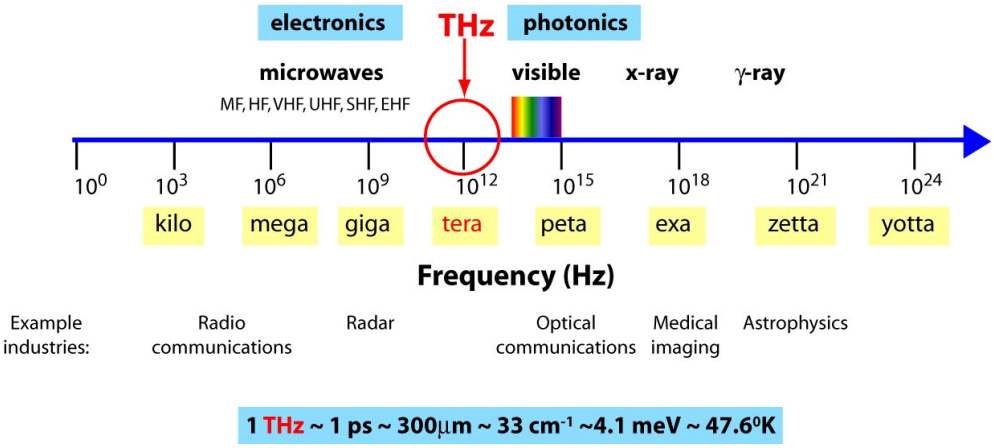

Figure 1. Schematic of the electromagnetic spectrum showing that THz light lies between electronics and photonics.

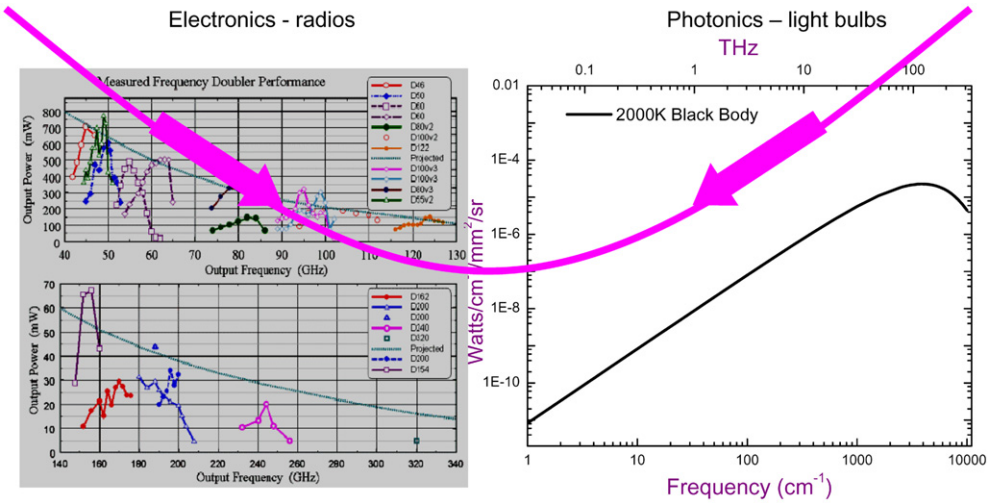

Figure 2. Illustration of the real THz gap—the decline in power as electronics goes to higher frequencies, and photonics goes to lower frequencies. Electronic data courtesy of Tom Crowe, Virginia Diodes Inc.

of the electric fields produced by them. In particular it will be seen that calculations for bunches containing many electrons and of electric fields in the near-field are of crucial importance.

In what immediately follows, we will discuss the evolution of what are essentially solutions of Maxwell's equations, which describe the physics behind the production of light from moving charges to expressions from which real numbers can be calculated of both power and brightness. It is important to realize that it is brightness, which is power per unit area per unit solid angle, and not just power, that make the sources described in this review paper, so useful. Brightness is at best conserved in an optical system, and thus more accurately describes on-sample, or per-pixel power, which usually governs signal to noise and hence the sensitivity of spectroscopy or imaging techniques. Power becomes important for highly absorbing samples and large area imaging.

At the simplest level, light is made from accelerating electrons. Associated with an electron is an electric field. A static electron has a static field that is radial, but if the electron is accelerated, a propagating field is generated. The situation is described by Maxwell's equation:

$$\nabla \times H = J_{\text{free}} + \varepsilon \frac{\partial E}{\partial t} + \frac{\partial P}{\partial t}, \tag{1}$$

where J_{free} is the current of free electrons, while the term on the left-hand side, and the middle term on the right-hand side are propagating fields. It is worth remarking that for an electron moving at a constant velocity, the field moves along with it, but does not propagate. Also note that we are not considering sources in which electrons jump between quantum levels nor are we considering light coming from changes in the polarizing field, given by the last term in equation (1), such as occurs in hot bodies or other more advanced schemes [11].

There have been many practical solutions to equation (1), and we will review them. However, in what follows initially (sections 2.1–2.3), we will deal with the situation for a *single electron*. Later we will consider the situation for a bunch of electrons and the reader needs to be clear of the differences. At the time of writing there is no single computation that takes full account of the emission from multiple electrons. To do so would require summing their electric fields paying attention to their individual positions and momenta and hence their relative phases in three dimensions.

2.1. Larmor's formula for total power

This is one of the simpler solutions, but is limited to calculations of the total power. However it is useful and instructive as we shall see. For a single electron [6, 7] it takes the form

$$\text{Power (W)} = \frac{2a^2e^2}{3c^3}(\text{cgs units}), \tag{2}$$

where a is the acceleration, e the charge on the electron, c the speed of light. Note again that there is no propagated power if the electron is moving in free space but not accelerating.

There is a major enhancement to the radiated power if the electron that is radiating has energies that are significantly higher than the electron rest mass energy of 0.5 MeV. A rather straightforward argument based on the dimensions of power (ML^2T^{-3}) can be used to show that in the relativistic electron case, the power emitted, given by equation (2), needs to be multiplied by γ^4, where γ is the ratio of the mass of the electron to the rest mass. Thus, in the particle frame, mass increases by γ, length reduces by γ and time dilates by γ, so that in the laboratory frame the Lorentz transforms have the result of increasing the power by γ^4, thus:

$$\text{Relativistic power (W)} = \frac{2a^2e^2}{3c^3}\gamma^4 \text{ (cgs units)}. \tag{3}$$

In particle accelerators which are used as light sources, γ typically ranges from 100 to several 1000 because the electron rest mass is 0.5 MeV and particle accelerators typically use beams that have energies from 10s to 1000s of megaelectronvolts. This is the main principle upon which synchrotron radiation sources work, at least in terms of power delivered. This principle also governs the spontaneous emission essential to the operation of FEL [12].

Applying this formula to a single electron, one obtains that for relativistic particles [13]

$$\frac{\mathrm{d}P}{\mathrm{d}\bar{\nu}} = 2.16 \times 10^{-25}\,\mathrm{J\,cm^1} \text{ per electron}, \tag{4}$$

which is seven orders of magnitude higher than the non-relativistic case. Here we note that the energy of the electron is irrelevant, since we quote the power per bandwidth. Higher energy electrons do yield higher total power as per equation (3), but into a correspondingly higher

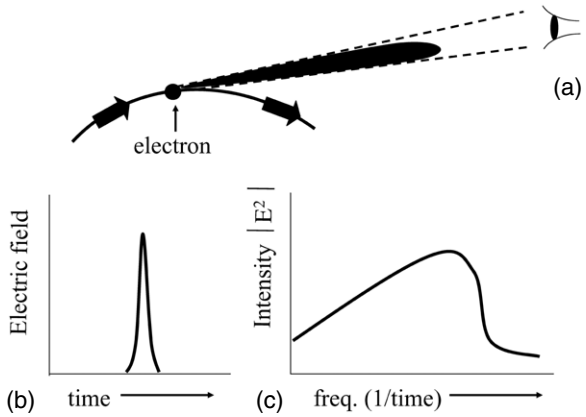

Figure 3. Schematic showing the physics of synchrotron radiation generation. An observer of an electron travelling in an arc in (*a*), 'sees' an electric field pulse (*b*), whose power spectrum is given by the Fourier transform (*c*).

bandwidth. In equation (4) P is the power emitted into an area $\times$ angle product approximately equal to the wavelength lambda. We will discuss this in detail in section 2.3.

Putting in some numbers, if the electron bunches contain 100 pC of charge, or 6.3×10^8 electrons, and anticipating the super-radiant effects dicussed in section 2.4, the power emitted will be

$$\text{Power emitted from } 100\,\text{pC} = 2.16 \times 10^{-25} \times (6.3 \times 10^8)^2 = 85\,\text{nJ cm}^1 \tag{5}$$

and thus we can quickly see that for a 100 MHz repetition rate, the power will be 8.5 W cm^1, or 850 W over a 3 THz (100 cm^{-1}) bandwidth.

2.2. Synchrotron radiation power

This treatment is based on an original 1949 paper by Schwinger [5], which was applied extensively to calculations of emission at x-ray wavelengths. All the early papers based on this paper were for x-ray wavelengths and took advantage of certain approximations relevant to short wavelengths. In the early 1980s Duncan and Williams [14] extrapolated the synchrotron calculations to the infrared and showed these sources to be 100–1000 times brighter than typical globar sources.

Synchrotrons are electron particle accelerators and they emit light via the mechanism shown in figure 3 [6, 7]. An electron in a magnetic field, accelerating around a bend and passing an observer produces a pulse of electric field as a function of time. The timescale for this event is attoseconds for most synchrotrons because the electrons are moving close to the speed of light. The spectral content of this pulse is obtained from the Fourier Transform of the modulus squared of the amplitude of the pulse. A broadband spectrum results. In practice 'bunches' of electrons circulate together in the accelerators but we defer detailed discussions of this until later.

Synchrotron radiation is not emitted into 4π sr like a blackbody source, but rather into a limited cone with a wavelength dependent opening angle of a few tens of milliradians [6–8]. This narrowing of the angle is due to relativistic effects, since the particles are travelling towards the observer at close to the speed of light and Lorentz transforms have to be applied. The light emission cone itself and the effective source area are functions of wavelength and

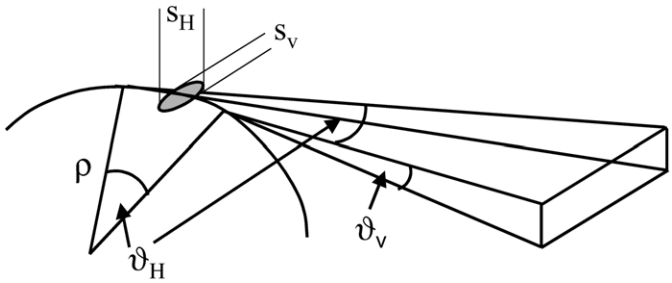

Figure 4. The geometry used to explain the physics of synchrotron radiation generation.

the collection geometry. We shall see that for each set of conditions there is a 'natural opening angle', $\theta_{\text{V-NAT}}$, which is one of the most useful concepts for synchrotron radiation emission in general, and is particularly useful in determining brightness.

Some terms will now be defined. With reference to figure 4, the source is an electron in a storage ring of energy E(gigaelectronvolts), and with a radius of ρ(metres). The horizontal and vertical angles of emission are θ_{H} and θ_{V}(radians), respectively. Similarly, assuming a Gaussian profile, the full width half maximum source size is defined as s_{H} and s_{V}(mm). We also have to introduce the concept of bandwidth, $\Delta\lambda/\lambda$ or $\Delta E/E$, and vertical angular increment $\Delta\theta_{\text{V}}$. Noting that mass and energy are equivalent, for electrons with a total energy, (m), of 1 GeV, which is much larger than the rest mass energy, (m_0), of 0.5 MeV, the velocity, which is given by $v/c = \sqrt{1-(m_0/m)^2}$ is about $0.999\,999\,97c$. Thus they will circulate around a 50 m circumference ring $c/50$, or 6×10^6, times per second, meaning that each electron will contribute $1.6 \times 10^{-19} \times 6 \times 10^6$ c s^{-1}. The number of electrons for one ampere of stored beam is thus $\sim 10^{12}$ rather than $\sim 10^{19}$. In a typical 9-bunch ring such as the National Synchrotron Light Source at Brookhaven [15], there are thus $\sim 10^{11}$ electrons per bunch, which is ~ 10 nC of charge. A 50 m circumference ring with 9 bunches will have a radio-frequency of 54 MHz, which is the pulse repetition frequency.

As we proceed with our calculations, we note that there is no consensus on the choice of units and the evolution of the field has been witness to the introduction of different expressions using different units. The main two units for power are photons per second and watts. Power in photons per second can easily be converted to watts by dividing P by $5.04 \times 10^{18} \times \lambda\,(\mu\text{m})$. The commonly used unit for wavelength is the micron, and the commonly used unit to describe the frequency or energy is cm^{-1}, which is the number of waves per centimetre. Wavenumbers convert to energy in millielectronvolts by dividing by 8. Thus, in these units, 1 THz is 300 μm or 33 cm^{-1}, or 4.1 meV. Thus 1000 cm^{-1} is equivalent to 10 μm wavelength, 100 cm^{-1} is equivalent to 100 μm and so on. The bandwidth chosen for most of the published formulae for photons per second is 0.1%, and this can fairly simply be changed to cm^{-1} if desired.

We begin the calculation with an evaluation of the total flux $F_{\text{total}}(\lambda)$ (photons per second or watts) emitted at a wavelength λ, into a bandpass $\Delta\lambda$, i.e. the integrated flux emitted in the wavelength range $\lambda-(\Delta\lambda/2)$ to $\lambda+(\Delta\lambda/2)$. It is important to note that the emission is isotropic horizontally since the beam sweeps around in this direction. Thus, we see immediately that $F_{\text{total}}(\lambda)$ will be linearly proportional to θ_{H}. Classical electrodynamics [6, 7] then gives the power emitted per electron, as a function of frequency (ω) and solid angle Ω:

$$\frac{\mathrm{d}^2 I}{\mathrm{d}\omega\,\mathrm{d}\Omega} = \frac{e^2\omega^2}{4\pi^2 c}\left(\int_{-\infty}^{\infty} \hat{n} \times (\vec{\beta} \times \hat{n}) \mathrm{e}^{\mathrm{i}\omega(t-((\hat{n}\cdot\vec{r}(t))/c))}\mathrm{d}t\right)^2, \tag{6}$$

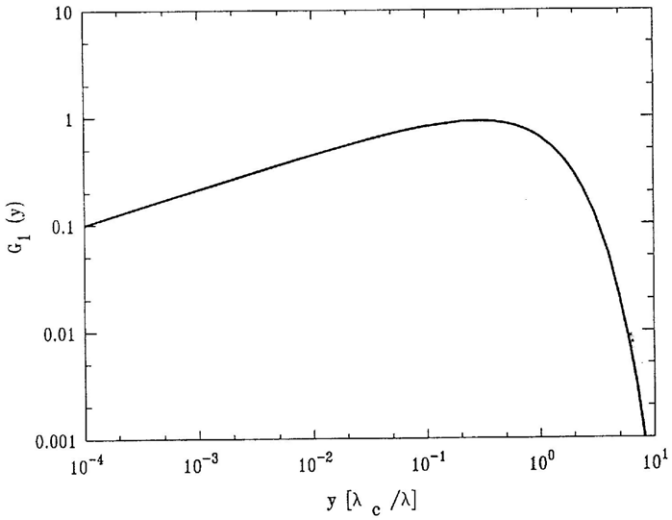

Figure 5. The $G_1(y)$ function used in the calculation of synchrotron radiation power. λ is the wavelength, and λ_c, the so-called critical wavelength defined in the text.

where $\vec{\beta}$ is the ratio of the velocity of the particle to the speed of light, $\vec{n}$ is a unit vector and $\vec{r}(t)$ is the particle position.

Kim [16] has shown that one can re-write equation (6) to give the total flux emitted in practical units, per horizontal milliradian per ampere into a 0.1% bandwidth ($\Delta\lambda/\lambda$ or $\Delta E/E$), integrated over θ_V as:

$$F_{\text{tot}} = 2.547 \times 10^{13} E(\text{GeV}) I(\text{A}) G_1(y) \text{ photons s}^{-1}, \tag{7}$$

where $G_1(y)$ is the Bessel function:

$$G_1(y) = \int_y^{\infty} K_{5/3}(\eta) \mathrm{d}\eta, \tag{8}$$

which is plotted in figure 5. In this expression $y = \lambda_c/\lambda$ where λ_c is the 'critical wavelength' given by [17]:

$$\lambda_c(\text{Å}) = \frac{5.59\rho(\text{m})}{E^3(\text{GeV})}, \tag{9}$$

which is that wavelength which bisects the power spectrum—i.e. half of the power is emitted at longer and half at shorter wavelengths than λ_c. The integral over the spherical fractional order Bessel function $G_1(y)$ can be readily evaluated using the algorithm of Kostroun [18], which states that

$$G_1(y) = 0.5\left(\frac{\mathrm{e}^{-y}}{2} + \int_{r=1}^{\infty} \mathrm{e}^{-y} \cosh(0.5r) \frac{\cosh(0.5kr)}{\cosh(0.5r)}\right), \tag{10}$$

where $k = 5/3$. In practice this is summed until the increment in $G_1(y)$ from an additional term in the series is $<10^{-5}$.

We note that the above is derived from the one electron calculation by multiplying by the total number of electrons. We will return to this in section 2.4.

The above expressions can be readily solved using a personal computer and we will now look at a numerical example. We will calculate the total flux emitted by the NSLS VUV ring at Brookhaven [15] at a wavelength of 10 μm (1000 cm^{-1}). We will assume that the ring is

operating at 0.75 GeV. The bending radius of this ring is 1.91 m and we will collect 100 mrad horizontally. Furthermore, a bandwidth of 0.1% or 1 cm^{-1} is assumed, which corresponds to evaluating the flux emitted from 999.5 to 1001.5 cm^{-1}. For this situation we find that using the expressions above, $F_{total} \approx 2.5 \times 10^{14}$ photons s^{-1} 0.1% bandwidth/A.

Another simple expression for the total power emitted in the infrared region in photons per second is

$$P(\lambda) = 4.38 \times 10^{14} \times I \times \theta_H \times \text{bw} \times (\rho/\lambda)^{1/3} \text{ photons s}^{-1}, \tag{11}$$

where I is the current in amperes, θ_H (rads) the horizontal collection angle, bw the bandwidth in per cent, λ the wavelength, and ρ the radius of the ring. λ and ρ are in the same units. Equation (11) gives the same answer as equation (7) and the above flux is equivalent to $\approx 5 \times 10^{-6}$ W cm^{-1} A.

2.3. Synchrotron radiation brightness

Brightness is sometimes called brilliance, or spectral radiance. For a given wavelength and bandwidth it has units of power per unit area per unit solid angle. In the previous section we evaluated the first term, and now address the angle and area terms.

Note that we will distinguish *power* in units of, say, watts, from *brightness*, in units of, say, watts per square centimetre per steradian. Brightness is an important quantity because it is at best conserved in any optical system, and it is usually what determines the sensitivity of an experiment because it determines the signal to noise in an infrared experiment via the formula

$$\%N = \frac{100A^{1/2}}{B(\nu)\Delta\nu\varepsilon t^{1/2}\xi D^*}, \tag{12}$$

where A is the detector area, D^* the detectivity of the detector, $B(\nu)$ the brightness, $\Delta\nu$ the bandwidth, ε the experiment's throughput, t the measuring time interval and ξ the optical efficiency. Properties of infrared detectors have recently been summarized by Richards [19]. The throughput, also called the etendue, is the product of the limiting area and angle of the experiment. Multiplying the brightness by the throughput yields the signal expected at the detector. For expression (12) to apply, the throughput must be less than the emittance, or (area × angle) product for the source!! We also note that a significant amount of effort in the development of this field has addressed fluctuations in $B(\nu)$, and that this is often an issue, but lies outside the scope of this review.

2.3.1. Emitted beam divergence—emitted flux versus angle. Here we are interested in calculating the emission at a fixed wavelength, λ into a 'vertical band' $\Delta\theta_V$ wide at θ_V, with $\theta_V = 0$ being defined as the orbit plane. The expressions $F_V(\theta_V)$ for the emission as a function of vertical angle can also be derived from equation (6) as shown by Krinsky [17] and by Hulbert and Williams [8]. Again we are interested in practical units and we find that

$$F_V(\theta_V) = 1.325 \times 10^{16} E^2 \left(\frac{\lambda_c}{\lambda}\right)^2 [((1+\gamma^2\theta_V^2)K_{2/3}(\zeta))^2 + \gamma^2\theta_V^2(1+\gamma^2\theta_V^2)K_{1/3}^2(\zeta)] \tag{13}$$

in units of photons per second per milliradian (horizantal) per milliradian (vertical) per ampere per 0.1% bandwidth. In the above equation, γ, defined earlier as the ratio of the electron mass to the rest mass, is given in practical units by

$$\gamma = 1957 \times E(\text{GeV}), \tag{14}$$

and ζ, the argument of the Bessel functions is given by

$$\zeta = \left(\frac{\lambda_c}{2\lambda}\right)(1+\gamma^2\theta_V^2)^{3/2}. \tag{15}$$

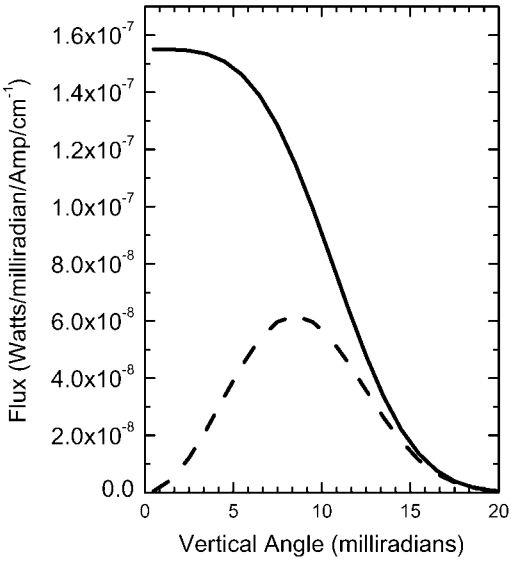

Figure 6. The calculated output spectrum as a function of vertical angle at 10 μm wavelength, for the NSLS, VUV ring at Brookhaven National Laboratory which has a bending radius of 1.91 m. The solid and dashed lines correspond to light polarized parallel to or perpendicular to the orbit plane.

The first term, in $K_{2/3}$, on the right of equation (13), represents light polarized parallel to the orbit plane (or horizontally polarized), while the second term involving $K_{1/3}$ corresponds to light polarized perpendicular to the orbit plane, (or vertically polarized). Clearly, we require the integral of $F_V(\theta_V)$ over θ_V in equation (13) to give the same answer as that obtained in the previous section. It is important to note that the expression is symmetrical about $\theta_V = 0$.

As in the previous section, equation (13) is readily evaluated using a personal computer and the algorithm of Kostroun [18]. Evaluating this for the same example as before, i.e. for the NSLS VUV ring [15] (1.91 m radius at 0.75 GeV) at 10 μm wavelength, we obtain the results that are plotted in figure 6. The behaviour at high values of θ_V, where the emission is essentially zero, indicates that we have chosen a large enough range for the given conditions.

In concluding this section we mention a result that can be derived from the long-wavelength limit of the synchrotron radiation emission equation. In the infrared, the vertical opening angle can be calculated from the simple formula [14]

$$\theta_{\text{V-NAT}}(\text{mrad}) = 1.66\left(\frac{1000 \times \lambda(\mu\text{m})}{\rho(\text{m})}\right)^{1/3}, \tag{16}$$

where $\theta_{\text{V-NAT}}$ is the angular range into which ~90% of the emitted photons travel. Using the above example for the NSLS VUV ring ($\rho = 1.91$ m) and $\lambda = 10\,\mu\text{m} = 10^5$ Å, we obtain $\theta_{\text{V-NAT}} = 27$ mrad, a reasonable result as confirmed from figure 6.

Thus we have shown how to completely characterize the emitted flux, including emission angles, for a given set of conditions, and specifically for one wavelength.

2.3.2. Horizontal source size. The other parameter that is required to calculate the brightness is the source area. We treat the horizontal and vertical components separately.

In general, there are three contributions to the horizontal source size and these are (1) the intrinsic size of the electron beam itself s_{Hi}; (2) the projected (observed) size due to the

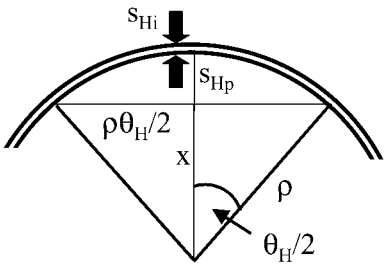

Figure 7. Illustration of the effect of a finite length of electron arc on a projected horizontal source size, S_{Hp}, for a synchrotron radiation source, for a horizontal angle of θ_H and for a bending radius of ρ. The intrinsic size S_{Hi} is shown by the thicker lines.

large horizontal angle and hence extended source s_{Hp}; and (3) the diffraction-limited source size s_{Hdiff}.

In the infrared region the intrinsic size is usually very small compared with other effects. This is illustrated in figure 7, in which it can clearly be seen that s_{Hp} is much larger than the intrinsic beam size, s_{Hi}. We can calculate s_{Hp} purely from geometrical considerations. Thus we have from figure 7

$$X \cong \sqrt{\frac{\rho^2 - \rho^2\theta_H^2}{4}}, \tag{17}$$

which can be re-arranged to give

$$X \cong \rho\left(1 - \frac{\theta_H^2}{4}\right)^{1/2}, \tag{18}$$

which is approximated by

$$X = \rho\left(1 - \frac{\theta_H^2}{8}\right). \tag{19}$$

Using $X + s_{Hp} = \rho$

$$s_{Hp} = \frac{\rho\theta_H^2}{8}. \tag{20}$$

This linear dependence of s_{Hp} on ρ is illustrated in figure 8 for four different radii. Much more dramatic, however, is the quadratic dependence of s_{Hp} on θ_H shown in figure 9. Here the source size is seen to quadruple when the angle θ_H doubles.

Finally, we can write the diffraction-limited source size as being given by λ/θ_H. The practical source size is then found by adding s_{Hi}, s_{Hp} and s_{Hdiff} in quadrature, thus $s_H = \sqrt{s_{Hi}^2 + s_{Hp}^2 + s_{Hdiff}^2}$.

If we substitute some numbers for the NSLS [15], $\rho = 1.91$ m and $\theta_H = 90$ mrad for the infrared extraction port built into the dipole chamber, we find that $s_{Hp} = 2$ mm. This is far larger than the intrinsic beam size which is 600 μm. s_{Hdiff} is a function of wavelength and for $\lambda = 100\,\mu$m, $s_{Hdiff} = 1.11$ mm. Note that when we move into the sub-THz range, for this geometry, for $\lambda = 1000\,\mu$m or 0.3 THz, then $s_{Hdiff} = 11.1$ mm!

2.3.3. Vertical source size. As for the case of the horizontal beam size, there are three contributions to the vertical beam size, s_V, which are the intrinsic size, s_{Vi}, the projected size,

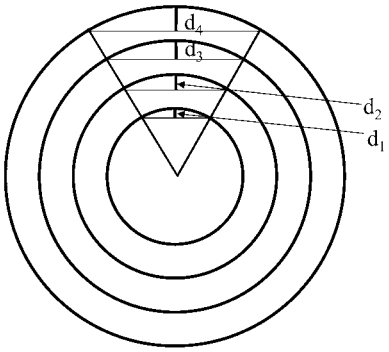

Figure 8. Illustration of the linear effect of increasing bending radius on the projected horizontal source size for a synchrotron radiation source.

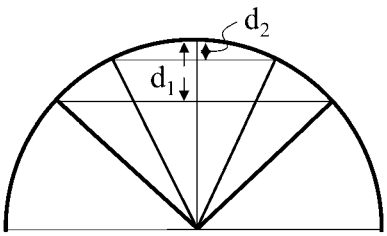

Figure 9. Illustration of the quadratic dependence of synchrotron radiation source size on horizontal angle.

s_{Vp}, and the size as a result of diffraction, s_{Vdiff}. Again the vertical size is dominated by the latter two.

Green [20] has made extensive calculations of the vertical source size, and these have been published in a paper by Williams [21]. However, it has been found in practice that a much simpler yet still accurate value for the vertical source size for horizontal angles around $\theta_{\text{v-NAT}}$, is obtained by analogy to the formula of equation (20), namely $s_{\mathrm{Vp}} = \rho\theta_{\mathrm{H}}\theta_{\mathrm{V}}/8$. Clearly the source size due to diffraction is given by $s_{\mathrm{Vdiff}} = \lambda/\theta_{\mathrm{V}}$, similar to the horizontal case.

Once again, putting in the numbers for the NSLS, with a vertical angle of $\theta_{\mathrm{V}} = 90\,\mathrm{mrad}$, we find with $s_{\mathrm{Vi}} = 0.2\,\mathrm{mm}$, we get $s_{\mathrm{Vp}} = 0.62\,\mathrm{mm}$ and for $\lambda = 100\,\mu\mathrm{m}$, or 3 THz, that $s_{\mathrm{Vdiff}} = 1.6\,\mathrm{mm}$.

In conclusion it is worth emphasizing that if the vertical or horizontal angles are set to be larger than $\theta_{\text{V-NAT}}$ the projected source sizes increase more rapidly than the gain in flux, resulting in a reduction in brightness. If the collection angles are smaller than $\theta_{\text{V-NAT}}$ the brightness is reduced due to increases in s_{vdiff} and s_{Hdiff}. However, assuming that the opening angles of the beamline match the synchrotron radiation natural opening angles, and assuming that the intrinsic source size is smaller than that due to diffraction, Jim Murphy [22] has shown that the brightness of synchrotron radiation is given for all rings by

$$B(\lambda) = 3.8 \times 10^{20} \times I \times \mathrm{bw}/\lambda^2\ \mathrm{photons/s/mm^2/sr}, \tag{21}$$

where again, λ is the wavelength in microns, I the current in amperes, bw the bandwidth in %.

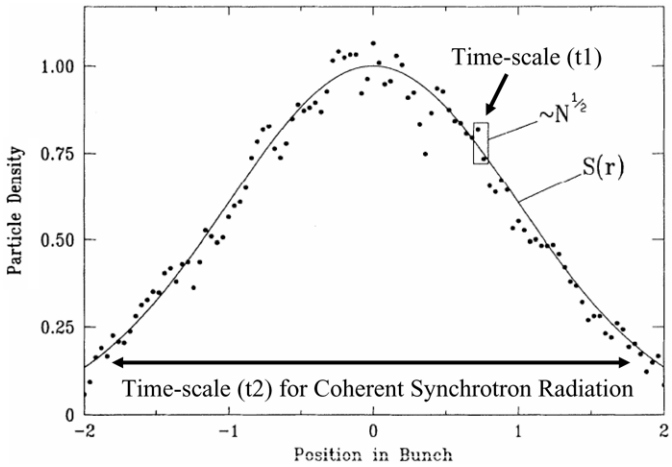

Figure 10. Illustration of a Gaussian statistical distribution of electrons in a bunch in an accelerator, and the two timescales. The timescale shown in the small rectangle is the one on which one can resolve the noise and gives the incoherent emission. The long timescale for coherent synchrotron radiation is that of the entire bunch.

2.4. Multiparticle effects and super-radiance

Just as significant as the gain in radiated intensity due to relativistic effects are those due to super-radiance or multiparticle coherent effects. To illustrate this effect we show a simulation of a real bunch of electrons in figure 10. This was generated using Monte Carlo techniques and is assumed to be Gaussian. It can be seen that there are two timescales, one given by the length of the entire bunch, and the other on the scale on which one can observe the statistical 'noise' on the bunch. The wavelength of the emitted light determines which timescale is relevant. For wavelengths short compared to the bunchlength, the length-scale of the noise applies. Thus strictly, the electric field for a bunch of electrons is $N^{1/2}$ times that of a single electron, so that the intensity is N times that of a single electron as mentioned in earlier remarks following equation (10), and indeed equations (7) and (10) are based on these assumptions.

For wavelengths that are longer than the bunchlength, the electric field is N times that of a single electron, and the intensity N^2 times the intensity of a single electron [7, 9, 10]. There is thus an enhancement factor proportional to N, the number of electrons. The basic physics of the situation is illustrated in figure 11. In figure 11(*b*), for example, two electrons radiate in phase together. In this case, the radiated power is four times that of the single electron shown in figure 11(*a*) because the field doubles. We saw in section 2.2 that typical electron bunches contain 100 pC to 10 nC of charge, so that this multiparticle coherent enhancement is 8–11 orders of magnitude.

In the case of multiple electrons, then, equation (6) must be multiplied [10] by the

$$\text{multiparticle coherent enhancement factor} = [N[1 - f(\omega)] + N^2 f(\omega)], \tag{22}$$

where N is the number of electrons, and $f(\omega)$ is the form factor, which is the Fourier transform of the normalized longitudinal particle distribution within the bunch, $S(z)$, and is given as follows:

$$f(\omega) = \left| \int_{-\infty}^{\infty} \mathrm{e}^{\mathrm{i}\omega\hat{n}\cdot\vec{z}/c} S(z)\,\mathrm{d}z \right|^2. \tag{23}$$

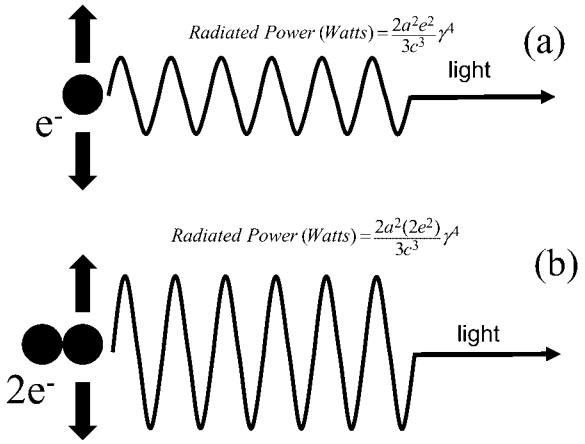

Figure 11. Illustration of Larmor's formula and in particular the quadratic dependence on the number of electrons, since (*b*) situation yields four times the radiated power of (*a*).

Such enhancement was first observed, studied and verified at several facilities, including linacs [23–26], compact waveguide FELs [27], and magnetic undulators [27–29]. It has recently been observed at storage rings [30–34] and at an energy recovered linac (ERL) [35], which will be described in section 3.

2.5. Exact solutions to the light emitted by electrons—the near-field and edge radiation

In the past sections we have described the development path of calculations to determine the power and brightness of light emitted from relativistic electron beams. These calculations are useful in giving a feel for the properties of the light via relatively simple calculations and concepts using approximations.

Recently, however, with the advent of more powerful computers and codes, exact solutions have become available. Significantly, no approximations are necessary and even more importantly, the new calculations deal with near-field effects that are particularly relevant to the THz part of the spectrum, and that have previously been ignored due to a far-field approximation in equation (6). The new calculations also allow the inclusion of the so-called edge effects, or the situation in which the electrons *enter* the magnetic field. In this situation the electrons experience a changing magnetic field as they enter the magnet, and the radiation pattern has a different symmetry and character than the synchrotron radiation emitted in the constant magnetic fields of the dipole magnets. Furthermore in the THz spectral region there are often interferences between radiation emitted from adjacent magnets, and this is also taken into account.

In what follows we discuss one of these codes [36], which happens to be the one we have worked successfully with. But we also note that there are many other codes, and that this is an active field at the moment.

The situation is handled theoretically as follows. First we present an exact formula for a single electron, and then generalize it to N electrons taking account of their longitudinal spatial distribution.

A so-called retarded potentials approach is used. This is a method of paying attention to the changing location of the moving charge with time, and hence launch point of the electric field and gives the exact expression for the frequency-domain electric field $\vec{E}_\omega$ generated by an

electron moving at $\vec{r}_e(\tau)$ with the relative velocity $\beta_e = c^{-1}\vec{r}_e$ (in the Gaussian cgs system) as

$$\vec{E}_\omega = \mathrm{i}ec^{-1}\omega \int_{-\infty}^{+\infty} [\vec{\beta}_e - [1 + \mathrm{i}c/(\omega R)]\vec{n}]R^{-1} \exp[\mathrm{i}\omega(\tau + R/c)]\mathrm{d}\tau, \tag{24}$$

where $\vec{r}(x, y, z)$ is the observer position, $R = |\vec{r} - \vec{r}_e|$ is distance from the electron to the observer, $\vec{n} = (\vec{r} - \vec{r}_e)/R$, ω is the radiation frequency. This is called the Lienard–Wiechart field [7]. At $\omega \neq 0$, equation (24) can be shown to be equivalent to the well-known expression of Jackson [6] by integration by parts

$$\vec{E}_\omega = ec^{-1} \int_{-\infty}^{+\infty} \frac{\vec{n} \times [(\vec{n} - \vec{\beta}_e) \times \dot{\vec{\beta}}_e] + cR^{-1}\gamma^{-2}(\vec{n} - \vec{\beta}_e)}{(1 - \vec{n}\vec{\beta}_e)^2 R} \exp[\mathrm{i}\omega(\tau + R/c)]\mathrm{d}\tau. \tag{25}$$

It is important to point out that equations (24) and (25) are exact expressions that take into account both near and far-field effects. A comparison with equation (6) shows that the so-called 'velocity' term that is multiplied by R^{-1} in the numerator was previously ignored. In the case of infrared synchrotron radiation, and THz radiation in particular, this term is not small and must be included in all calculations.

To illustrate near-field effects taking place in the case of emission from one and two dipole magnet edges, we give approximate relations obtained from equation (25) at short distances. For the hypothetical case of a relativistic electron moving along a straight line ($x_e = y_e = 0$) from $-\infty$ and entering the dipole magnet at the longitudinal position $z_e = 0$, with the observer located at the longitudinal position z, downstream from the dipole magnet edge, and within the limits $\lambda \ll z \leqslant \lambda\gamma^2$, the intensity as a function of distance away from the axis S, is:

$$\left.\frac{\mathrm{d}F}{\mathrm{d}S}\right|_{1nf} \approx \alpha \frac{\Delta\omega}{\omega} \frac{4I}{e\pi^2} \frac{\sin^2[\pi\kappa^2/(2\lambda z)]}{\kappa^2}, \tag{26}$$

where λ is the radiation wavelength, α the fine structure constant, I the current and $\kappa = (x^2 + y^2)^{1/2}$, $\kappa \ll z$.

Equation (26) predicts a ring structure with the radius of the first ring of the order of $\kappa_{nf} \approx (\lambda z)^{1/2}$. We note that the product of this value and the apparent divergence of the radiation beam in this case appears clearly larger than the minimal value allowed by the diffraction limit, which is $\kappa_{nf}^2/z > \lambda/(4\pi)$.

In the case of two adjacent dipole magnets whose edges are separated by a distance L, under conditions of validity of equation (26), we obtain

$$\left.\frac{\mathrm{d}F}{\mathrm{d}S}\right|_{2nf} \approx \alpha \frac{\Delta\omega}{\omega} \frac{4I}{e\pi^2} \frac{\sin^2[\pi\kappa^2 L/[2\lambda z(z + L)]]}{\kappa^2}, \tag{27}$$

which is in agreement with equation (26) for $L \ll \lambda\gamma^2$, if the argument of the sine is $\theta = \kappa/[z(z + L)]^{1/2}$. This predicts an interference pattern superimposed on the ring structure of equation (26). We note that the relations $L \ll \lambda\gamma^2$ and $\lambda \ll z \leqslant \lambda\gamma^2$ are well satisfied in most cases for storage rings and linacs used as light sources in the middle- and far-infrared spectral range.

Going to the far field, Bosch [37] has computed expressions for a single edge as

$$\frac{\mathrm{d}F}{\mathrm{d}\Omega} = \alpha \frac{\Delta\omega}{\omega} \frac{I}{e\pi^2} \frac{\gamma^4\theta^2}{(1 + \gamma^2\vartheta^2)^2}, \tag{28}$$

and for two edges as:

$$\left.\frac{\mathrm{d}F}{\mathrm{d}\Omega}\right|_2 = \left.\frac{\mathrm{d}F}{\mathrm{d}\Omega}\right|_1 \left|1 - \exp\left[\frac{\pi L}{\lambda\gamma^2}(1 + \gamma^2\theta^2)\right]\right|^2, \tag{29}$$

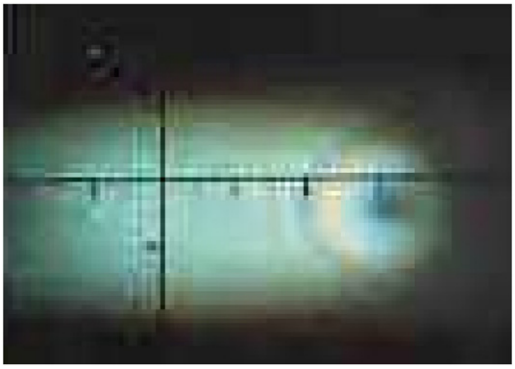

Figure 12. Photograph of edge radiation at Daresbury laboratory [37]. In particular note the circle on the right-hand side.

which can be reduced to

$$\left.\frac{\mathrm{d}F}{\mathrm{d}\Omega}\right|_2 \approx \left.\frac{\mathrm{d}F}{\mathrm{d}\Omega}\right|_1 \sin\left[\frac{\pi L}{2\lambda\gamma^2}(1+\gamma^2\theta^2)\right]^2. \tag{30}$$

Edge radiation differs from synchrotron radiation in being radially polarized. It is also emitted into narrower angles than synchrotron radiation, which, when considerations of basic wave optics are introduced, imply a source area of $\lambda\gamma$ [13].

The calculational techniques to determine E for various magnetic structures for a single electron that we have used have been developed by Chubar and Elleaume [36]. This code is called the synchrotron radiation workshop (SRW). At the time of writing, the calculations can also allow for bunches of electrons of finite emittance, but not finite length, so that calculations based on equation (25) must be multiplied by the enhancement factor determined by equations (22) and (23). However, the SRW code will eventually incorporate multielectron emission including proper handling of the electron beam emittance. We note for the record that in the accelerator physics community this coherent synchrotron radiation is the subject of deep study, but as yet, not in a way that has yielded practical numerical solutions for our community.

The phenomenon of edge radiation, including interference effects, was studied in the late 1970s in the Soviet Union [38, 39]. A photograph of the type of pattern obtained was published on the cover of the 1984 annual report [40] of Daresbury Laboratory in the UK in the early 1980s, and one of these images is reproduced in figure 12. In this figure, the ring structure is evident on the right, with synchrotron radiation emission on the left. Subsequently much theoretical work was done by Bosch [41], and a beamline at the Aladdin storage ring in Stoughton, Wisconsin, USA, was constructed to extract and deliver edge radiation and utilize it for microspectroscopy. Groups at BESSY, Berlin Germany [42], at LURE, Orsay, France [43] and at the ESRF in Grenoble, France [44] also got engaged in the topic. Beamlines at the ANKA storage ring in Karlsruhe, Germany [45], at the ESRF [44] and at Jefferson Lab in Newport News, Virginia, USA [46] all currently deliver edge radiation and several others are planned such as the Soleil facility in France, and the Australian Synchrotron Project in Melbourne, Australia.

Dumas and Chubar in particular have pioneered applications of the SRW code to infrared beamlines, including wavefront propagation, for their own and several other facilities, and their result for the Jefferson Lab facility at 1 THz is shown in figure 13. In particular one can

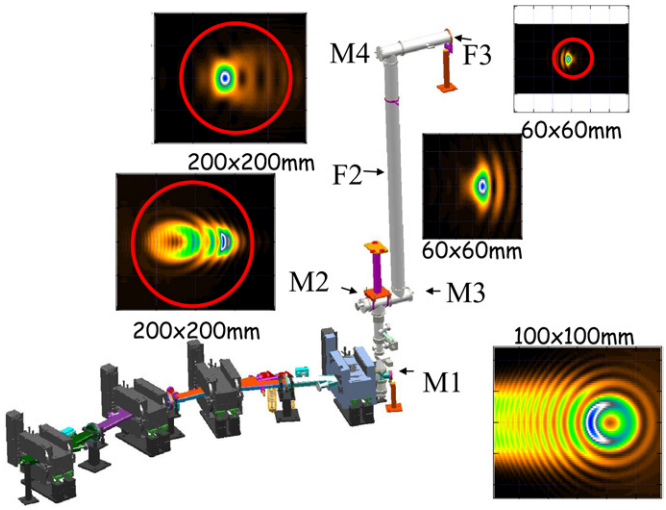

Figure 13. Schematic of the Jefferson Lab high power THz beamline, showing in particular calculations of the emitted and propagating field using the SRW code. The dimensions of the screens are shown, while the circles represent the sizes of the optical components.

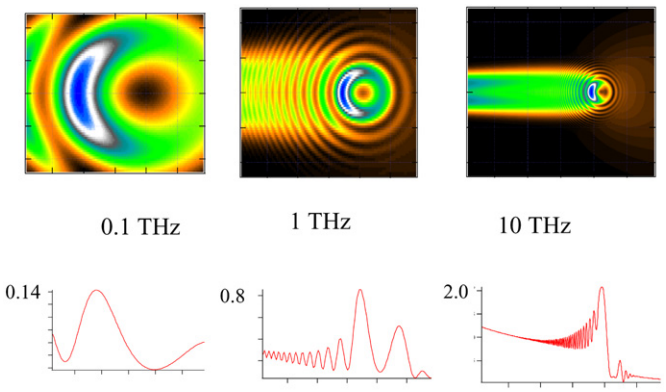

Figure 14. Top: calculated output power distribution on the first mirror of the Jefferson Lab high power THz beamline, showing the strong changes in opening angle as a function of the frequency. The boxes are 100 mm × 100 mm. Bottom: horizontal cuts through the distributions showing the fringes from interference of two edges, and increasing to the left, the normal synchrotron radiation term. Units for the latter are 10^9 photons/s/0.1% bandwidth/mm^2.

compare the calculated intensity on the first mirror, shown at the lower right of the figure, with that observed at Daresbury in figure 12.

We can also look at the wavelength dependence of the emission, which was discussed before and is given approximately by equation (16). Calculations for the intensity distributions on the first mirror, M1, are shown in figure 14 for 0.1, 1.0 and 10.0 THz. The patterns are dominated by the interference pattern from the edge radiation from two magnet edges; however, the synchrotron radiation is clearly visible as two stripes, particularly on the 10 THz figure. It can also be seen in the horizontal cuts. For different wavelengths striking changes in the patterns are evident. Finally, we note that since M1 is at 625 mm from the source point, these are all in the near-field.

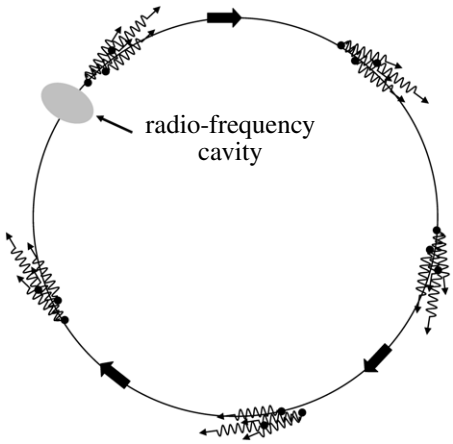

Figure 15. Schematic of a synchrotron radiation source.

3. Accelerators

In this section we will discuss the development of accelerators that have been built as light sources. We will accompany the description by presenting typical performance numbers which pertain to, and reveal clearly, the evolution of brighter, or more powerful light sources. The distinction between brightness and power will be dealt with later, both being important descriptors of light sources.

Electrons that are at relativistic energies radiate when accelerated according to equation (3). A large number of light sources around the world have been built to exploit this property. Light which is generated in this way is called synchrotron radiation, since it was first observed in electron synchrotrons. The accelerators themselves can be conveniently classified into generations. Thus, first generation light sources operated parasitically on electron synchrotrons that were built for particle physics. Second generation light sources were based on electron storage rings, which run at higher average currents than was affordable on synchrotrons, where the electron beam was injected, accelerated and dumped many times per second. Third generation storage rings are similar to second generation ones with the addition of long straight sections for specialized magnetic structures called wigglers or undulators, which will be described later. The electron beams also have a lower emittance. Finally, a new generation of light sources has been developed based on energy storage rings, called ERLs [47–49], in which electrons circulate only once, allowing them to be bunched more tightly both laterally as well as longitudinally, yielding even lower emittance electron beams with sub-picosecond pulse lengths.

A schematic of a second generation storage ring is shown in figure 15. Electrons are contained in bunches so that the energy lost due to radiation can be restored in a radio-frequency (rf) cavity. In most storage rings the electron orbit is not circular, but comprises bends induced by dipole magnets, with short straight sections in between. This is shown in the photograph (figure 16) of the second generation, 750 MeV storage ring, built in 1981 as part of the National Synchrotron Light Source [15], at Brookhaven National Laboratory. In the photo, the large dipole bending magnets are clearly visible, with smaller multipole focusing magnets in between in the straight sections. In a ring such as this, the bunchlength is related to the rf cavity frequency which is typically in the 50 to 500 MHz range, yielding bunchlengths from a few 100 ps to a few 10s of ps. In figure 16, the rather large 50 MHz rf cavity is the horizontal cylinder with one face towards the camera, at the left of the picture.

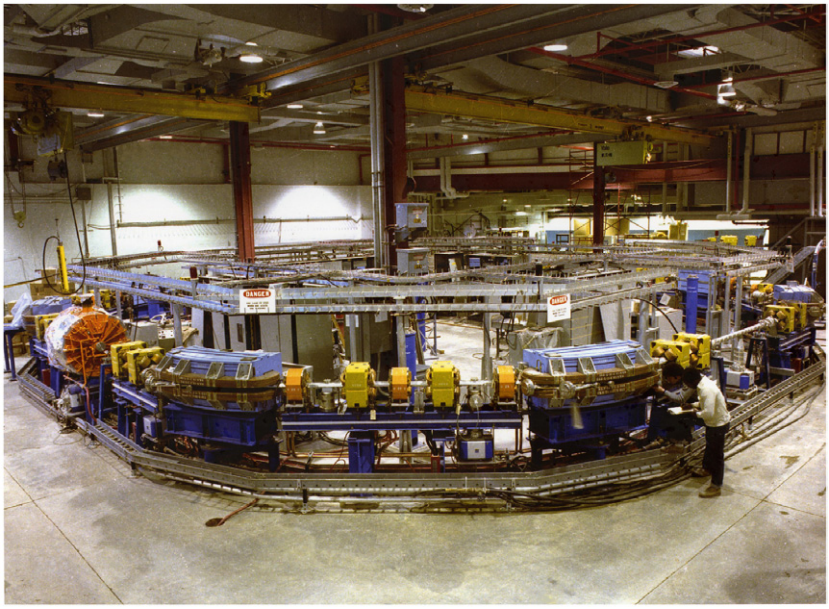

Figure 16. Photograph of the NSLS UV/IR synchrotron radiation source at Brookhaven National Laboratory.

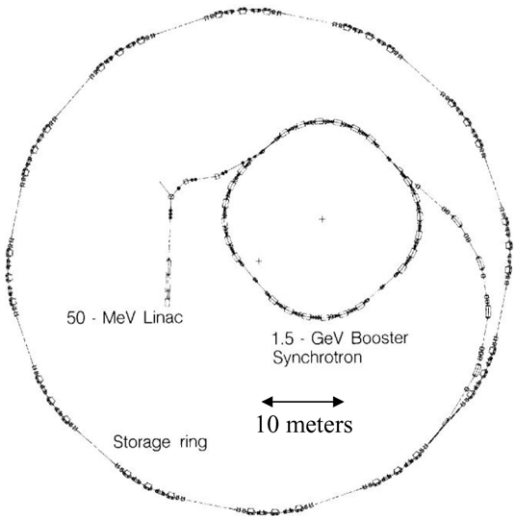

Figure 17. Plan of the Advanced Light Source at Lawrence Berkeley National Laboratory.

Third generation sources, as mentioned earlier, are storage rings with long straight sections in which wigglers or undulators, which are devices containing multiple alternating dipole fields, are placed. As an example we show in figure 17, a schematic of the Advanced Light Source at Lawrence Berkeley National Laboratory, in the USA [50]. Note that the bending and focusing magnets are arranged such as to leave long straight sections available, unlike the ring pictured in figure 16. In the long straights are placed devices with multiply alternating fields called undulators or wigglers [7, 50], depending on the strengths of their magnetic fields. Higher

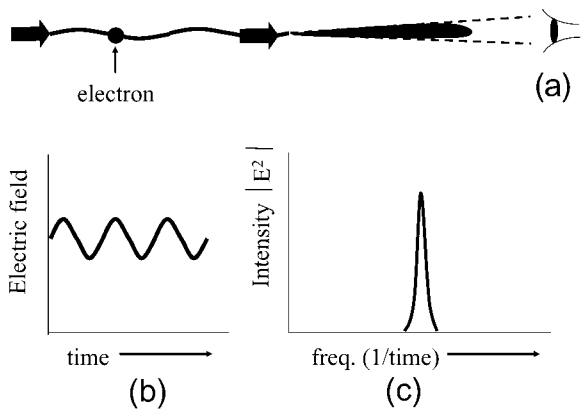

Figure 18. Schematic showing the physics of the generation of light from undulators or wigglers. An observer of an electron travelling along the undulating path in (*a*), 'sees' an electric field as in (*b*), whose power spectrum is given by the Fourier transform (*c*).

field devices are called wigglers, and in these the electron path contains large deviations such that there is no temporal coherence between the radiation emitted from adjacent wiggles. The radiated power thus increases due to the increase in the length over which the light is being radiated. Several texts have described the behaviour of these devices [51]. Here we are interested mainly in the concepts, and for this we show in figure 18, what happens in the situation in which the electron path is sinusoidal (*a*) as would be the case for an undulator. The electric field is itself sinusoidal (*b*), and the Fourier transform is then a narrow function (*c*), but is considerably enhanced at the special frequency. Relating back, the broadband spectrum of figure 3(*c*), is basically compressed by a factor depending on the number of periods, but typically 100, with a corresponding increase in power and brightness at that one wavelength.

Now that we have introduced undulators and multiparticle coherence, we note that both can be combined, which is the situation at the THz facility at UC Santa Barbara [3], and more recently at the Budker Institute of Nuclear Physics in Novisibirsk, Russia [52]. We have seen that to accomplish multiparticle coherence, the electrons have to be separated by a distance that is less than the wavelength of light being emitted. This can be achieved in the following way. An optical cavity is placed around the undulator. In this case the spontaneous emission from the first electrons to pass the device, is reflected back and forth, so that subsequent electrons find themselves in both electric and magnetic fields while travelling in the undulator. If conditions are right, the resulting ponderomotive force has the effect of micro-bunching the electron beam on the scale of the wavelength. The situation just described is the FEL [12], and it can be achieved using either storage rings or linacs. The physics of the situation that we have just described is illustrated in [10], and reproduced in figure 19. The figure also illustrates that such a device can simultaneously produce THz light as mentioned earlier.

Moving towards fourth generation light sources, the thrust is towards ever lower emittance electron beams, meaning primarily that the electron beams are packed more tightly both longitudinally and transversely. The equilibrium emittance of storage rings is primarily determined by the balance of radiation damping and quantum excitations. Lower emittance than this can be obtained, by definition, by going into a non-equilibrium regime. One way of achieving high THz output is to operate electron storage rings [30–34] under special conditions in which radiation emitted from the back of the bunch, catches up with the front and modifies the electron spatial distribution, so that multiparticle coherent emission enhances the THz output. Not all the electrons contribute to the coherent THz emission in this case, and low beam current

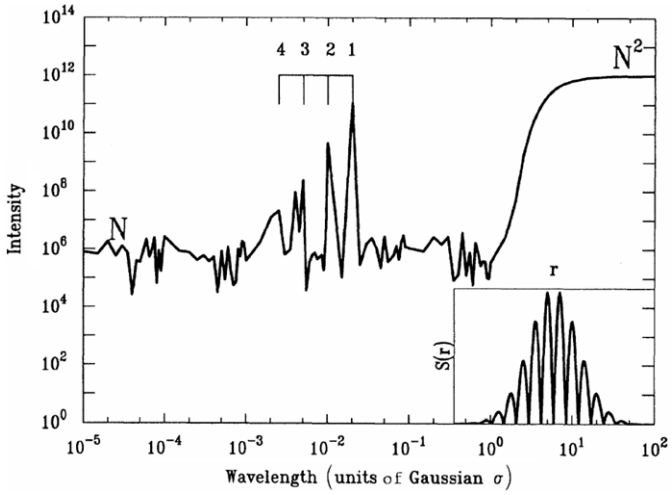

Figure 19. Illustration of the calculated emission from a statistical Gaussian bunch of 106 electrons, which is modulated according to the distribution shown in the inset. This represents the situation in a FEL [10].

is usually necessary. Another way to lower the emittance is to use linacs [23–29] to create tightly packed bunches of electrons, to induce them to emit light, and then to discard them. In this latter case, all the electrons do contribute to the coherent THz emission. However, to reproduce the typical electron beam conditions found in a storage ring source with an energy of 1 GeV, and a current of 100 mA, would require 100 MW of power. Such linac-based sources therefore typically operate at low duty factors. A solution is to recover the energy of the electrons prior to discarding them [47]. To date this technique has yielded much higher power. It is accomplished in, for example, the Jefferson Lab Free Electron Laser facility [48, 49], figure 20, and in the Budker Institute Accelerator-Recuperator project [52], by using what is called an Energy Recovered Linac, or ERL.

The Jefferson Lab machine uses a superconducting linac and is really, then, an energy storage ring, rather than an electron storage ring. Unlike room temperature linacs, the superconducting one can run continuously with very little loss. The bunches of electrons are created by the photoemission process using a short-pulsed laser, and start life immediately in a high density regime. They are accelerated using rf linacs that are superconducting, and hence which have minimal losses. The electron bunches circulate only once, and return to the linac out of phase, thus giving up their energy. The energy is temporarily stored in the superconducting structure of the linac before being quickly utilized by a subsequent new bunch emitted from the gun. In this accelerator, the electron beam energy is up to 160 MeV, with each electron bunch carrying 135 pC of charge at bunch repetition frequencies of up to 75 MHz. The device produces hundreds of watts of broadband THz light as the electrons pass a magnetic chicane prior to the optical cavity of an IR or UV FEL.

The Budker Institute Accelerator–Recuperator [52] uses a normal conducting linac in energy recovered mode to drive an optical cavity-based FEL which operates 12 MeV electron bunches at 11 MHz, and with a bunch charge of around 1 nC. The device produces around 1 kW of average power, narrow band but tunable THz light.

Finally we note, given the numbers just quoted, that this triumph of accelerator engineering, namely the ERL, has all the properties we need for filling the THz gap at high peak and average power. The high repetition rate, combined with a modest charge per bunch,

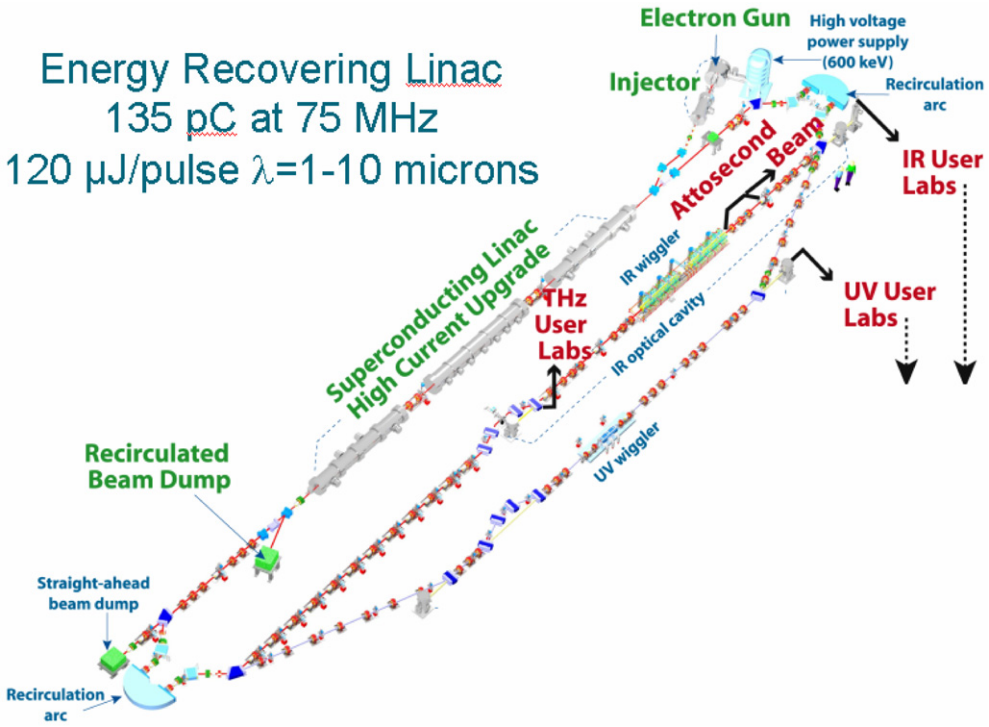

Figure 20. Artists impression of the FEL facility at Jefferson Lab, which is based on an ERL.

at relativistic energies, and emitting super-radiantly, yields a THz source that is many hundreds of watts of average power, and megawatts of peak power.

Let us look, then, at a series of calculations representing the THz output that represents a culmination of the evolution of the field. We have chosen to do this generically, by picking parameters that are very similar to, but not exactly the same as, those found at modern accelerator facilities. The parameters are, however, bound by reasonable limits. For the calculations we assume a 100 MHz repetition rate. In figure 21 we show the THz power spectrum for a series of pulse widths for a bunch charge of 100 pC. This keeps the current at the 10 mA level. In figure 22, we show the effect of different bunch charges on the output of 100 fs long bunches at 100 MHz. As mentioned before, 1 nC of charge has already been achieved at the Budker Institute [52] and also at Stanford [53] and Brookhaven [13], the latter two at low repetition rates, meaning lower average power. At Jefferson Lab, 10 mA of average current has been run.

In terms of brightness, the power calculated above and shown in figures 21 and 22, is emitted into a phase-space, or area × angle product, that is very close to the diffraction limit. The angles are of the order of 100 mrad, which means that the diffraction limited source size at 1 THz would be 3 mm, which is larger than the electron beam in most machines.

If we now take the Budker Institute THz resonator, then the power and brightness at a given wavelength are enhanced because the radiated path is longer, and thus the spectrum is narrower according to figure 18. Enhancements are typically in the range 100–1000 for a given bunch charge.

Finally, we note that there are presently several programmes in place [53] that plan to build ERLs as light sources, including Cornell and Florida State Universities in the USA, and the

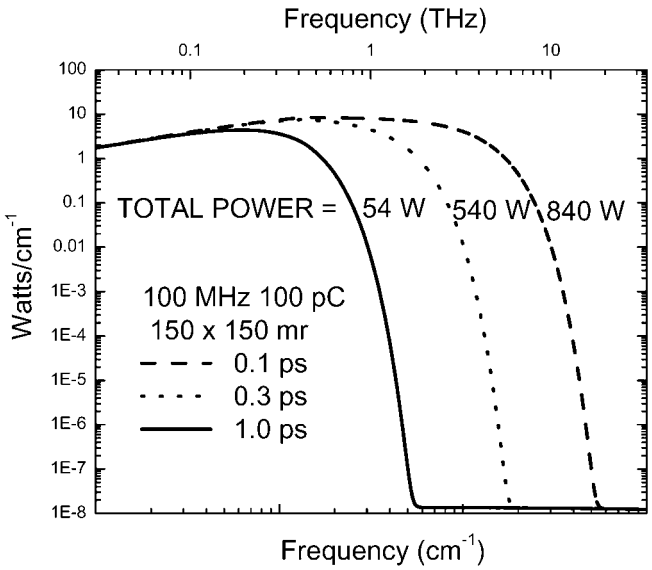

Figure 21. Calculated THz emission from a coherent synchrotron radiation source, showing the power spectrum and integrated power for 100 pC bunches at 100 MHz and different bunch lengths. The collection angle is 150 × 150 mr.

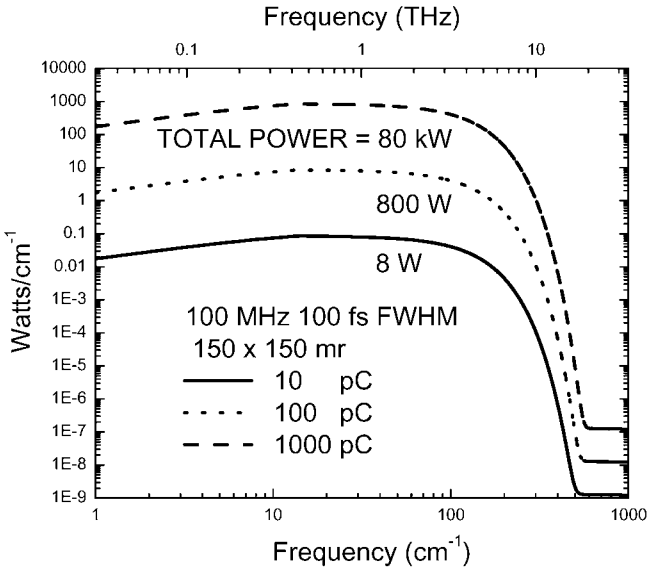

Figure 22. Calculated THz emission from a coherent synchrotron radiation source, showing the power spectrum and integrated power for 100 fs FWHM bunches at 100 MHz and different bunch charges. The collection angle is 150 × 150 mr.

4GLS project at Daresbury Laboratory in the UK. The quest for many are currents of 100 mA or higher, and this is an accelerator frontier. Bunches of higher charge have the effect that their induced image charges tend to cause what is called beam breakup, which considerably reduces the emittance and efficiency of the energy recovery process.

4. Applications of high power THz sources

We can only scratch the surface here, as the topic of this section covers many fields from biology and medicine to chemistry, physics and materials science. It is also a rapidly evolving field that is currently in its infancy. However, a fundamental understanding of the properties of materials requires measurements in the THz range because many important dynamical phenomena, from protein collective vibrational modes to superconducting bandgaps, involve this energy or frequency range.

Our familiar world is dominated by energy transport and flow. It affects all material behaviour including physics, chemistry and the biology and quality of life. Thus it is important to understand energy pathways—how leaves capture and store the energy of sunlight, for example, or how muscles capture and utilize oxygen. Energy can exist chemically in bonds, in atomic vibrations as heat or in electrons as currents. Measurements of the dynamical properties of materials, both in and out of equilibrium, then, are essential tools for probing the links between the quantum-electrodynamics based theoretical models of physical properties of materials and the physical properties themselves. In particular the dynamical interplay between atomic motion via vibrational modes or phonons, and the electronic system, appears to be a particularly strong governing factor. Such coupling, is, incidentally forbidden by the Born–Oppenheimer relationship, since the light electrons, strongly coupled by the electromagnetic force, are assumed faithfully to follow nuclear motions.

High power THz, though, has two distinct niches—namely imaging and spectroscopy, the latter using multiple photons in a new regime of high electric fields. For the former, one can readily calculate that if 500 μW of power images 1 cm^2 in 5 min, then 100 W would image 667 cm^2 s^{-1}, a number that might make it valuable for large-scale security or medical screening. This might be useful since THz light can pass through clothing, paper, cardboard, wood, masonry, plastic and ceramics and because the wavelength corresponds to some biomolecular vibrations, it might be possible to identify certain materials such as explosives or bio-terrorism agents via their spectral characteristics.

For spectroscopy using the new generation of THz sources, the interest is in non-equilibrium dynamical measurements using multiple photons. The very high electric fields of up to 10^9 V m^{-1}, with half-cycle pulses, offer fantastic opportunities for creating Rydberg states by applying an impulse to a shallow bound electron. An early utilization of the concomitant magnetic fields to study dynamics of magnetism has been reported [54].

5. Conclusions

The new generation of low emittance accelerators, using ultrashort (sub picoseconds) bunches of electrons at relativistic energies, all provide high power THz light. They, therefore, mark a watershed in the development and utilization of this spectral range, a range that is rich in potential and novel applications. At the time of writing there are many missing concomitant factors which if not developed will impede progress in this area. The most critical are the lack of a THz camera and the lack of experimentally based human tissue exposure standards. Thus, at present, high power THz sources are not deployable except in class 4 laser enclosures, and furthermore, even if they were deployed for imaging purposes, there are no cameras to capture the images. There also is a paucity of filter manufacturers, though there is excellent knowledge from the astronomy community on how to build them.

All of this means that the development of the field will follow an interesting path with many interleaving component developments. Nevertheless, the potential of the field, is, in the author's opinion, likely to have at least as large an impact as, for example, the synchrotron based

protein crystallography experiments that are so popular at the time of writing. Ultimately it is likely that scientific enquiry will want to go beyond static structure to kinetics and dynamics, and THz sources and instrumentation should be ready to serve when that time arrives.

Acknowledgments

The development of infrared synchrotron radiation over the past 30 years or so has involved several 100 people. Among them I am particularly grateful to Larry Carr, Yves Chabal, Oleg Chubar, Fred Dylla, Paul Dumas, William Duncan, Carol Hirschmugl, Fritz Hoffmann, Dieter Moeller, Jim Murphy, George Neil, and to the NSLS beamline group at Brookhaven and the FEL team at Jefferson Lab. In my development of infrared facilities, I have enjoyed many helpful interactions with Takao Nanba, Jack Yarwood, Derek Martin, Paul Richards, Al Seivers and David Tanner. My research over the period has been funded primarily by the Division of Basic Energy Sciences, US Department of Energy and by the US Department of Defense.

References

[1] Auston D H, Cheung K P, Valdmanis J A and Kleinman D A 1984 *Phys. Rev. Lett.* **53** 1555
[2] Kohler R *et al* 2002 *Nature* **417** 156
[3] Ferguson B and Zhang X-C 2002 *Nature Mater.* **1** 26
[4] Ramian G 1992 *Nucl. Instrum. Methods* A **318** 225
[5] Schwinger J 1949 *Phys. Rev.* **75** 1912
[6] Jackson J D 1975 *Classical Electrodynamics* (New York: Wiley)
[7] Brau C A 2004 *Modern Problems in Classical Electrodynamics* (New York: Oxford University Press)
[8] Hulbert S L and Williams G P 2001 *Handbook of Optics: Classical, Vision, and X-Ray Optics* vol III, 2nd edn ed Bass M *et al* (New York: McGraw-Hill) p 32.1
[9] Dicke R H 1954 *Phys. Rev.* **93** 99
[10] Hirschmugl C J, Sagurton M and Williams G P 1991 *Phys. Rev.* A **44** 1316
[11] Ardavan A *et al* 2004 *J. Appl. Phys.* **96** 7760
[12] Brau C A 1990 *Free Electron Lasers* (San Diego: Academic)
[13] Carr G L 2003 private communication
[14] Duncan W D and Williams G P 1983 *Appl. Opt.* **22** 2914
[15] van Steenbergen A and NSLS Staff 1980 *Nucl. Instrum. Methods* **172** 25
[16] Kim K J 1989 *AIP Conf. Proc.* **184** 565
[17] Krinsky S, Perlman M L and Watson R E 1983 *Handbook of Synchrotron Radiation* ed E E Koch (Amsterdam: North Holland) chapter 2
[18] Kostroun V 1980 *Nucl. Instrum. Methods* **172** 371
[19] Richards P L 1994 *J. Appl. Phys.* **76** 1
[20] Green G K 1977 *Brookhaven National Laboratory Report* 50595
[21] Williams G P 1982 *Nucl. Instrum. Methods* **195** 383
[22] Murphy J B 1998 private communication
[23] Nakazato T *et al* 1989 *Phys. Rev. Lett.* **63** 1245
[24] Happek U, Blum E B and Sievers A J 1991 *Phys. Rev. Lett.* **67** 2962
[25] Wang D X, Krafft G A and Sinclair C K 1998 *Phys. Rev.* E **57** 2283
[26] Lihn H-C, Kung P, Settakorn C and Wiedemann H 1996 *Phys. Rev. Lett.* **76** 4163
[27] Doria A, Bartolini R, Feinstein J, Gallerano G P and Pantell R H 1993 *IEEE J. Quantum Electron.* **QE-29** 1428
[28] Jaroszynsky D A, Bakker R J, van der Geer C A J, Oepts D and van Amersfoort P W 1993 *Phys Rev. Lett.* **71** 3798
[29] Berryman K W, Crosson E R, Ricci K N and Smith T I 1996 *Nucl. Instrum. Methods* A **375** 526
[30] Tamada H, Tsutsui H, Shimoda K and Mima K 1993 *Nucl. Instrum. Methods* A **331** 566
[31] Abo-Bakr M *et al* 2003 *Phys. Rev. Lett.* **90** 094801-1
[32] Andersson A, Johnson M S and Nelander B 2000 *Opt. Eng.* **39** 3099–105
[33] Arp U *et al* 2001 *Phys. Rev. ST Accel. Beams* **4** 54401-1
[34] Carr G L 2001 *Nucl. Instrum. Methods* A **463** 387

[35] Carr G L *et al* 2002 *Nature* **420** 153
[36] Chubar O, Elleaume P 1998 *Proc. EPAC98 Conf.* (Stockholm, 22–26 June 1998) p 1177
[37] Bosch R A 1999 *Nucl. Instrum. Methods* A **431** 320
[38] Nikitin M M *et al* 1979 *Sov. Phys.—JETP* **52** 388
[39] Nikitin M M, Medvedev A F and Moiseev M B 1981 *IEEE Trans. Nucl. Sci.* **NS-28** 3130
[40] *Annual Report* 1984/85 Daresbury Laboratory, Warrington, Cheshire, UK
[41] Bosch R A, May T E, Reininger R and Green M A 1996 *Rev. Sci. Instrum.* **67** 3346
[42] Schade U *et al* 2000 *Nucl. Instrum. Methods* A **455** 476
[43] Mathis Y-L *et al* 1998 *Phys. Rev. Lett.* **80** 1220
[44] Dumas P *et al Intl. J. Infrared Millim. Waves* submitted
[45] Mathis Y-L, Gasharova G and Moss D 2003 *J. Biol. Phys.* **29** 313
[46] Greer A *et al Opt. Soc. Am.* submitted
[47] Tigner M 1965 *Nuovo Cimento* **37** 1228
[48] Neil G *et al* 2000 *Phys. Rev. Lett.* **84** 662
[49] Benson S *et al* 2004 *FEL Conf. Proc. (Trieste)* **229** www.JACoW.org
[50] Robinson A L and Schlacter A S 1990 *Nucl. Instrum. Methods* A **291** 499
[51] Winick H 1994 *Synchrotron Radiation Sources* (Singapore: World Scientific)
[52] Vinokurov N A *et al* 2004 *Proc. 2004 FEL Conf. (Trieste)* p 226
[53] Corneliussen S 2005 *CERN Courier* **45** 26
[54] Tudosa I *et al* 2004 *Nature* **428** 831